Artical ID:1006-3471(2012)04-0348-11

Electrochemical Performances of Layered Polypyrrole/Chemically Reduced Graphene Oxide Nanocomposites as Supercapacitor Electrodes

XU Si-zhe, ZHOU Xue-jiao, WU Kun, YANG Yong-qiang, WU Hai-xia*

(*Research Institute of Micro/Nano Science and Technology*, *Shanghai Jiao Tong University*, *Shanghai* 200240, *China*)

Abstract: Nanocomposites of polypyrrole (Ppy) and chemically reduced graphene oxide (CRGO), Ppy/CRGO, have been fabricated through *in-situ* polymerization of pyrrole on graphene oxide (GO) sheets. The as-synthesized Ppy/CRGO composites were characterized complementarily using scanning electron microscopy (SEM), thermogravimetric analysis (TGA) and Fourier transformed infrared spectroscopy (FT-IR). By controlling the initial ratio of the GO to pyrrole, the layered composites could be obtained and their thickness could be tuned properly. The Ppy/CRGO electrodes were prepared using a mechanical compressing technique and their electrical conductivity and electrochemical properties were characterized systematically. We demonstrated that as electrodes for supercapacitor, the Ppy/CRGO composites with Ppy to CRGO mass ratio of 10:1 showed a competitive capacitance of 421 $F \cdot g^{-1}$ that could be further increased to 509 $F \cdot g^{-1}$ by introducing pores in it, which is higher than that of Ppy alone. Given the manifest electrical and electrochemical properties, we envisage that the Ppy/CRGO composites should find applications in supercapacitors.

Key words: graphene oxide; chemically reduced graphene oxide; polypyrrole; composite; supercapacitor

CLC Number: O631; TB332; TM53 **Document Code**: A

The renewable energy source exploration and energy storage technology development have attracted great attentions during last few decades[1-5]. The energy storage technology has been considered as one of the key factors for industrializing the renewable energy resources[6-7]. As one of the mainly used energy storage devices, supercapacitor has been widely used in high power pulsed lasers, electric vehicles, digital telecommunication systems, uninterruptible power supply for high power devices[6,8-9], owing to their advantages of short charging time, long cycle life, thermal stability, energy reversibility and high power capacitance[9-11]. Generally, the supercapacitors can be divided into two categories according to the energy storage mechanisms. One is the electrical double-layer capacitor (EDLC), in which the energy is stored by the ions being absorbed on the interface between the electrode (such as high-area carbon material) and the electrolyte[7,9-10]. The other is the pseudocapacitor, in which the energy is stored through redox reaction at the surface and internal of the electrode materials[7,9,12]. Due to the redox reaction conducted in the electrode, the cycle life and capacitance stability of pseudocapacitor remain to be improved[13].

Besides the high electrical conductivity and de-

Received: 2011-12-26, Revised: 2012-02-21 * Corresponding author, Tel: (86-21)34206233, E-mail: haixiawu@sjtu.edu.cn
This work was supported by the National Natural Science Foundation of China (No. 20906055), National "973 Program" (No. 2010CB933900) and the State Key Laboratory of Bioreactor Engineering (No. 2060204)

cent stability, the ideal electrode material for supercapacitor should have exceptional capacity[13]. Several carbon materials, such as activated carbons[14-16], mesoporous carbons[17-18], carbon nanotubes[16,19-20] and graphene[10,21], have been used as electrode materials for supercapacitors, but the poor mechanical property (fragmented easily) is their drawback for practical applications[17,22]. Conducting polymers, such as polyaniline[23-24], polypyrrole[25-26] and polythiophene[27], have also been employed as electrode materials of supercapacitor with enhanced mechanical strength over the carbon materials, but their capacities and the stability are relatively lower[6,13,28-29]. Consequently, in order to produce an electrode with high capacitance, good cycling stability and excellent mechanical strength, the composites of carbon materials and conducting polymer have been explored. For example, using graphene/Ppy composite coated on glass carbon or Pt electrodes, the capacitors with the capacitances of 482 $F \cdot g^{-1}$ at a current density of 0.5 $A \cdot g^{-1}$, and of 267 $F \cdot g^{-1}$ at the scan rate of 0.1 $V \cdot s^{-1}$ have been reached[6,13].

In this work, layered composites of Ppy and chemically reduced graphene oxide (CRGO) have been synthesized simply through *in-situ* polymerization of pyrrole on the graphene oxide (GO) sheets. Two kinds of the Ppy/CRGO electrodes, the solid ones and the porous ones, were prepared. The morphologies and properties of as-synthesized Ppy/CRGO composites and the electrodes were characterized. It was demonstrated that the as-prepared porous electrodes showed the competitive capacitance of 509 $F \cdot g^{-1}$ at a scan rate of 0.005 $V \cdot s^{-1}$.

1 Experimental

1.1 Materials

Graphite (crystalline powders, ~ 500 mesh) was purchased from Shanghai Yifan Company (Shanghai, China). $NaNO_3$, $KMnO_4$, pyrrole monomer and ammonium persulfate (APS) were purchased from Sinopharm Chemical Reagent Co., Ltd. Ethanol, HCl and H_2SO_4 were acquired from Shanghai Lingfeng Chemical Reagent Co., Ltd. (Shanghai, China). GO was prepared through a procedure described previously[30-31].

1.2 Synthesis of Ppy/CRGO Composite

Ppy/CRGO composites were prepared through an *in-situ* polymerization procedure. The pyrrole monomer was pre-purified by distillation under vacuum to remove impurities. In a typical experiment, 10 mg GO was dispersed in 40 mL of H_2O by ultrasonication, then 104 μL (100 mg) of purified pyrrole monomer was added into the GO suspension in an ice bath, and then stirred for 30 min. Finally, 10 mL of APS (34%, by mass) was slowly added into the mixture, and it was observed that the suspension turned immediately from transparent to black. The reaction mixture was continually stirred for 30 min. The solid product was separated by filtration, washed alternately by ethanol and distilled water, each for 3 times, to remove the excess pyrrole monomer and APS, and dried finally under vacuum for 12 h at 40 ℃. Through the same procedure, the composites with the initial pyrrole to GO ratios of 100∶1, 50∶1, 10∶1, 5∶1, 3∶1 and 2∶1 in weight were prepared, and named as PG100, PG50, PG10, PG5, PG3 and PG2, respectively. Meanwhile, for comparison, pure Ppy was also prepared using the aforementioned procedure.

1.3 Preparation of Electrode

To prepare solid Ppy/CRGO electrodes, typically, 5 mg Ppy/CRGO was pressed into a circle wafer of 6 mm in diameter under a pressure of 2.5 MPa. Then, one side of the wafer was painted with silver conductive adhesive, and at the same time, a thin copper wire was connected onto it. Additionally, a passive layer (Epoxy) was deposited on the silver conductive adhesive and copper wire. The Ppy electrode was prepared with the same method.

To prepare the porous Ppy/CRGO electrodes, the Ppy/CRGO was mixed with microsized $CaCO_3$ particles and ground completely. Subsequently, the mixture was pressed into a wafer of 6 mm in diame-

ter under 2.5 MPa. The wafer was incubed in 1 mol · L^{-1} HCl for 12 h to remove $CaCO_3$ and washed by distilled water 3 times to remove the residual Ca^{2+} and Cl^-.

1.4 Characterizations

The morphologies of composites and electrodes were characterized using FESEM (Zeiss ultra 55, Germany) operated at an accelerating voltage of 2.0 kV. The FT-IR spectra were acquired on an EQUINOX 55 FT-IR spectrometer (Bruker, Germany). The specimens for FT-IR measurement were prepared by grinding the dried powders of Ppy/CRGO composites and KBr together, and then compressed into thin pellets under 20 MPa. TGA analysis was performed on TG209 F1 Thermogravimeter (ZETZSCH, Germany). A heating rate was set to 10 ℃ · min^{-1} and the analytical temperature region was from 30 to 800 ℃. The BET of the electrodes were measured on ASAP 2020 automatic surface area and porosity analyzer (Micromeritics, USA).

1.5 Electrochemical Property Measurements of the Ppy/CRGO Composite Electrode

The electrical conductivity measurement of the Ppy/CRGO composite electrodes was conducted on a SZ-82 digital four-point probe system (Suzhou, China). Cyclic voltammetry (CV), galvanostatic charge-discharge curves and electrochemcial impedance spectra (EIS) were measured on a CHI 660C three-electrode electrochemical workstation (Shanghai, China) equipped with a Ag/AgCl as the reference electrode and a platinum wire as the counter electrode. The electrolyte was 2 mol · L^{-1} H_2SO_4 aqueous solution. The CV curves were scanned from 0.005 V · s^{-1} to 0.1 V · s^{-1} within −0.2 ~ 0.45 V. The galvanostatic charge-discharge tests were carried out at the current density between 0.25 A · g^{-1} and 5 A · g^{-1}. The EIS was recorded under the frequency range from 0.01 Hz to 100 kHz.

The capacitance of the single cell can be calculated from:

$$\text{Capacitance}(C_m) = \frac{I\Delta t}{\Delta V m} \quad (1)$$

or

$$\text{Capacitance}(C_m) = \frac{S}{v \cdot \Delta V m} \quad (2)$$

where I is the constant current, Δt is the discharge time, ΔV is the interval between the highest and the lowest scanning voltages, m is the mass of composite in the electrode, S is the area of current-potential curve in CV test, and v is the potential scan rate. The energy density and power density can then be evaluated based on the following equations:

$$\text{Energy density}(E_m) = \frac{C_m V^2}{2} \quad (3)$$

$$\text{Power density}(P_m) = \frac{E_m}{t} \quad (4)$$

where V is the largest voltage range that the electrode can reach and m is the mass of the sample.

2 Results and Discussion

2.1 Characterizations

The Ppy/CRGO composites were prepared by *in-situ* polymerization of the pyrrole on GO. The FESEM images of pure Ppy, GO and Ppy/CRGO composites are shown in Fig. 1A ~ F.

The pure Ppy assumes a typical spherical morphology with a diameter about 300 nm (Fig. 1A). The particles are agglomerated due to physical fusing or the crossing polymerization among the particles. The original GO used in the work shows unique two dimensional (2D) layered structure. More interestingly, as shown in Fig. 1C ~ F, the morphologies of the Ppy/CRGO composites depend strongly on the initial ratios of pyrrole to GO. When the ratio of pyrrole to GO was 100∶1 (Fig. 1C), the composite appeared to have spherical morphology similar to that of the pure Ppy. The reason might be that the concentration of GO in the reactant is too low to affect the polymerization of pyrrole monomers. When the ratio of pyrrole to GO decreased to 50 and 10, the Ppy/CRGO composites with 2D layered structure were obtained (Fig. 1D and 1E). The thicknesses of the composite layer are of 27 nm and 12 nm, which are much thicker than that of the original GO sheets[30]. This result implies that the Ppy was poly-

merized on the GO surface. As the ratio of pyrrole to GO was further decreased, the as-generated composites still maintained a layered motif (Fig. 1F), but the agglomerated GO sheets were obtained. In this case the Ppy formed on the GO surface, but the layer was not thick enough to prevent the stacking of GO. For comparison, we also conducted the parallel polymerization using the pre-reduced GO sheets (called also CRGO), but no Ppy was formed on the pre-reduced GO (Fig. 2).

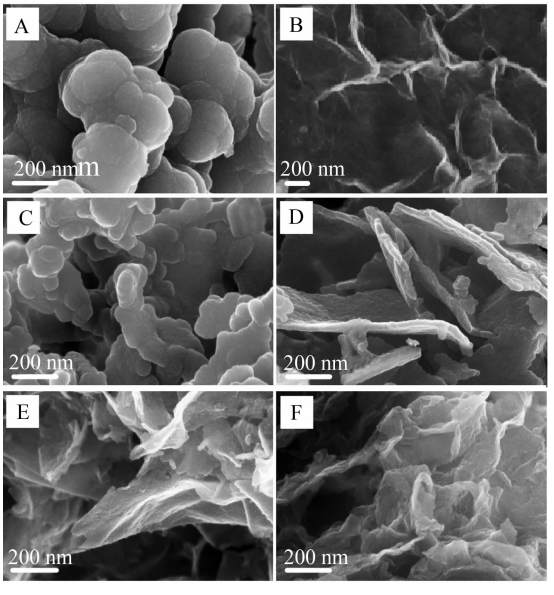

Fig. 1　FESEM images of pure Ppy (A), GO (B), PG100 (C), PG50 (D), PG10 (E) and PG5 (F)

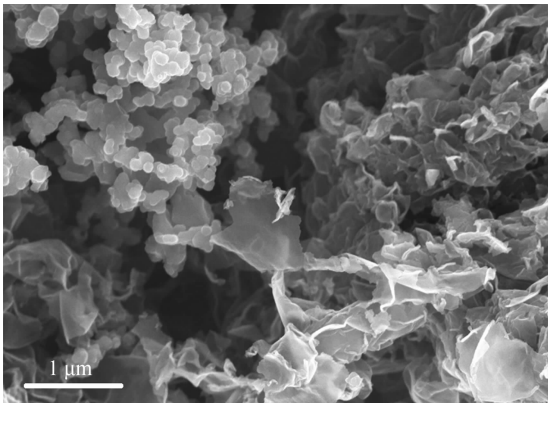

Fig. 2　SEM image of Ppy/CRGO composite prepared through the polymerization of pyrrole in the presence of pre-reduced GO (called also CRGO)

2.2　Interactions Between Ppy and GO

To get insight into the interactions between Ppy and GO, FTIR spectra of the as-prepared composites were acquired and are compared with those of the GO and Ppy in Fig. 3A. As shown in Fig. 3A, before the formation of the Ppy on it, the stronger C═O stretching vibration band (1726 cm^{-1}), O—H vibration band (1411 cm^{-1}), and C—O stretching band (1050 cm^{-1}) could be observed on the FTIR spectrum of the GO[30]. With the formation of the layered composites (named as PG10, 10 indicates the value of ratio of pyrrole to GO), the aforementioned typical vibration bands related to the oxygen-containing groups of the GO disappeared. Meanwhile, several new bands at 1557, 1192, 1045 and 915 cm^{-1} appeared, which are close to those of the stretching vibrations of pyrrole rings and the C—N stretching vibrations of pyrrole at 1553, 1189, 1042 and 913 cm^{-1}[32], but shifted a little bit to higher wavenumbers. These results indicate that during the formation of the composites, some of the oxygen-containing groups of GO have been removed (GO is reduced to CRGO). Considering that the pyrrole molecule could be used as a reductant[33], the reduction of the GO to CRGO should be possible.

The interaction between the Ppy and CRGO was further verified by TGA analysis. As shown in Fig. 3B, because the evaporation of the absorbed water, Ppy, GO and Ppy/CRGO showed a mass loss, ~2%, at around 65 ℃. For pure GO sheets, 13% of mass loss at 214 ℃ was detected, corresponding to the removal of the oxygen-containing groups from the surface of GO. The carbon backbone of GO was completely degraded at 515 ℃. For the pure Ppy, 7% of mass was lost at 249 ℃, but 22% of its mass was still maintained at 800 ℃. For composite PG10, the TGA showed clearly that it is not a physical mixture of the CRGO and Ppy. It should be noted that at 168 ℃, only 3% of its mass was lost, and probably due to the removal of the residual oxygen-containing groups on the CRGO. The mass loss at 245 ℃ related to Ppy decomposition was observed. Different from the GO and Ppy, at 800 ℃,

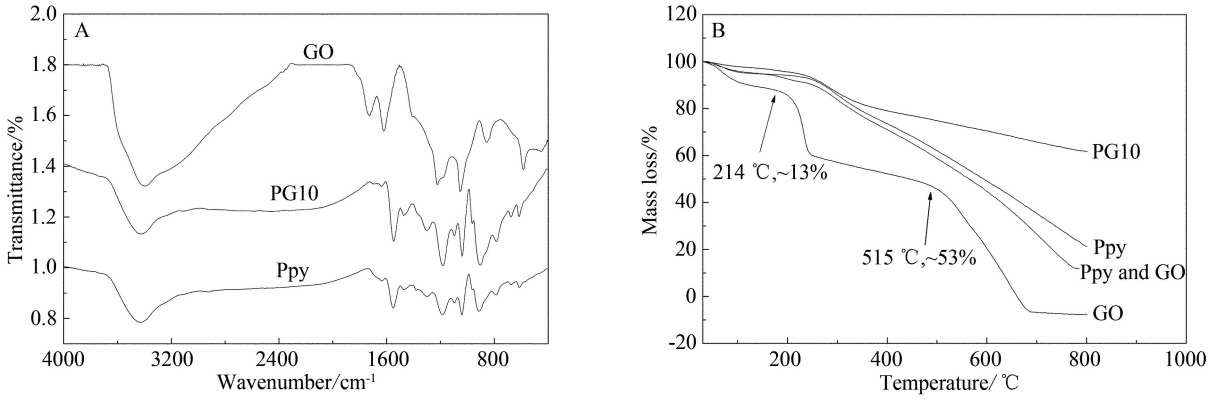

Fig. 3 FT-IR spectra (A) and TGA spectra (B) of pure Ppy, GO and PG10

62% of mass of PG10 composites are still remained, showing that it is much more stable than the individual Ppy and GO. This demonstrates further that the Ppy molecules are not physically loaded on the CRGO. To verify this, physically blended individual Ppy and GO with the same mass ratio of 10∶1 was prepared and its TGA spectrum was acquired under the same condition. As shown in Fig. 3B, the thermal stability of physical blends is much poorer than that of the as-prepared layered composites.

2.3 Electrochemical Performance of the Ppy/CRGO Electrodes

The conductivities of the solid electrodes for Ppy, GO and Ppy/CRGO composites are shown in Fig. 4. The pure Ppy shows a conductivity of 0.76 $S \cdot cm^{-1}$, and GO has no detectable electrical conductivity[34-35]. In comparison, the Ppy/CRGO composites showed much higher conductivity, for example, the PG10 composite has the conductivity of 5.19 $S \cdot cm^{-1}$.

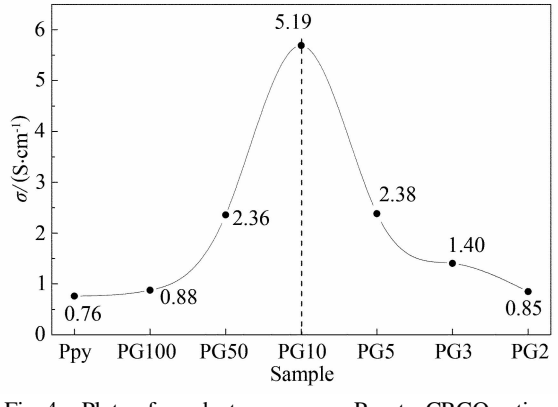

Fig. 4 Plots of conductance versus Ppy to CRGO ratios in Ppy/CRGO composites

The cyclic voltammetry, galvanostatic charge-discharge test and electrochemical impedance spectra were also used to determine the electrochemical performance of the electrodes prepared using Ppy/CRGO composites. As depicted in Fig. 5A, a nearly rectangular and symmetric current-potential response (CV curve) was acquired using PG10 composite electrode, illustrating the excellent reversible stability and ideal capacitive properties. It can also be seen that there is no redox peaks in the scan potential range between −0.2 and 0.45 V, indicating that it is an EDLC. As the scan rate increases, the area of CV curves also increases, suggesting that the PG10 electrode should have great power efficiency. However, in comparison, the capacitance of PG10 composite electrode, 359 $F \cdot g^{-1}$, is smaller than that of Ppy electrode, 421 $F \cdot g^{-1}$, shown in Fig. 5B. Galvanostatic charge-discharge curves obtained at a current density of 1 $A \cdot g^{-1}$, as seen in Fig. 5C, further verified it. Obviously, the discharging rate of PG10 electrode is slower than that of the pure Ppy. The reason might be that the PG10 composite has layered motif, therefore, when high pressure was applied to compress the powder into the solid electrode, the composite layers could be stacked much more densely than the spherical Ppy, which may affect the electron diffusion within the PG10 composites. This could be further verified by EIS test results, shown in Fig. 5D. The Nyquist plot of PG10 electrode shows a straight line with a slope near to 1 at the low frequency region and a small semicircle curve in the high frequency region.

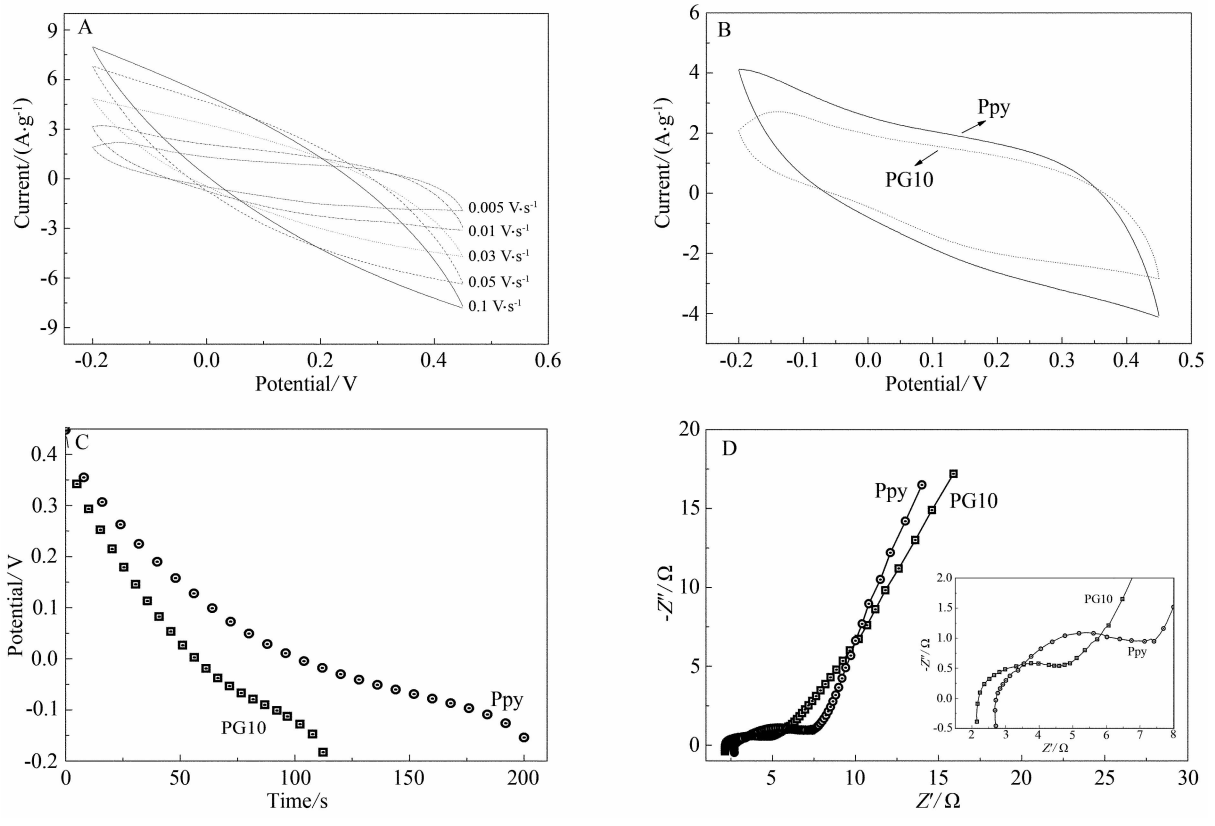

Fig. 5　Electrochemical performance of the electrodes prepared using Ppy/CRGO composites

A. CV curves of the solid PG10 composite electrode acquired via various scan rates from 0.005 V · s^{-1} to 0.1 V · s^{-1}; B. CV curves of solid PG10 and pure Ppy electrodes obtained at scan rate of 0.01 V · s^{-1}; C. galvanostatic charge-discharge curves of solid PG10 and pure Ppy electrodes measured at current density of 1 A · g^{-1}; D. Nyquist plots of PG10 and pure Ppy electrodes

The diameter of semicircle curve in high frequency region represents the electronic transmission between interfaces of electrode materials. The larger semicircle illustrates that the electrode has a higher interfacial resistance, which may be raised by the poor conductivity of the electrode materials[29]. The intercept of semicircle at the real axis is the equivalent series resistance (ESR), determining the charged/discharged rate of the supercapacitor. The straight line at lower frequency region is corresponding to the ion diffusion in the electrolyte[7]. Usually, the slope of the straight line at lower frequency region reflects the capacitive behavior of the electrode[29,36]. From Fig. 5D, the diameter in Nyquist curve of PG10 is much shorter than that of Ppy, implying that the conductivity of PG10 electrode is higher than that of Ppy, which is in agreement with the above conductivity measurement results. The nearly 45° slopped straight line of PG10 implies that lots of obstacles must be in ion diffusion path length resulting in the increase of obstruction of ion movement, which might be a main reason for the lower capacitance of PG10 compared with that of Ppy.

The contact area between the electrode and electrolyte plays an important role in the ion diffusion in EDLC. To maximally use the high surface area of the layered Ppy/CRGO composites in the electrodes, the porous electrodes were prepared by mixing certain amount of microsized $CaCO_3$ in the composites, which was degraded after the electrodes were compressed using HCl. The surface morphologies of as-prepared porous electrodes were examined using FESEM and are shown in Fig. 6A ~ D. The porous ratio could be tuned by control on the amount of $CaCO_3$ in the mixture. In this work, the mass ratios of $CaCO_3$ to PG10 varied from 0.5∶1, 1∶1, 2∶1, and the corresponding

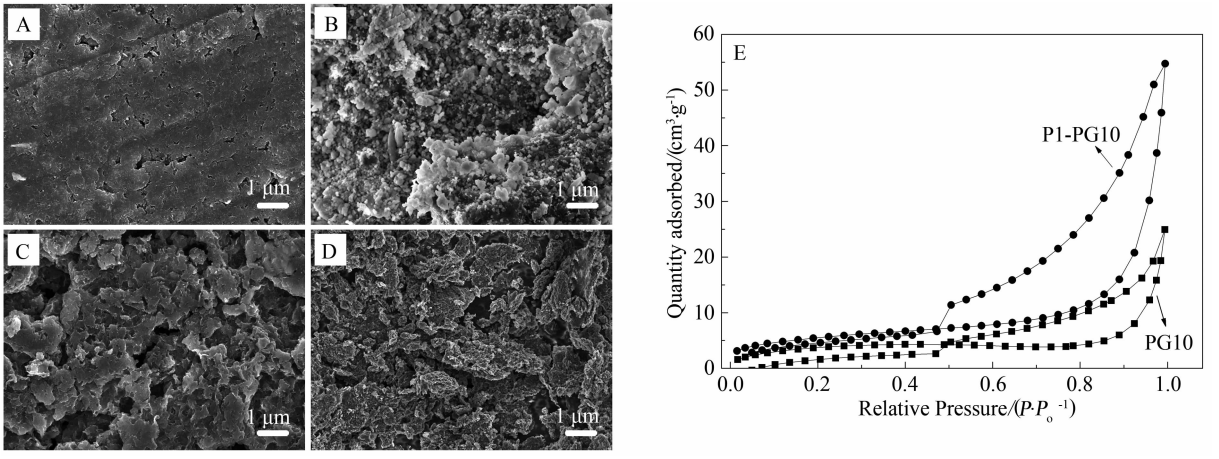

Fig. 6 FESEM images of solid PG10 electrode (A), a wafer of the compressed mixture of PG10 and $CaCO_3$ particles (B), porous PG10 (P1-PG10) electrode prepared by removal of the of $CaCO_3$ (C), porous P2-PG10 electrode (D), and Nitrogen adsorption isotherms of PG10 and P1-PG10 electrodes (E)

electrodes prepared were named as P0.5-PG10, P1-PG10 and P2-PG10. The BET data of solid PG10 and P1-PG10 electrodes are 14.6 $m^2 \cdot g^{-1}$ and 19.9 $m^2 \cdot g^{-1}$, among which the micropore areas account for 11.5 $m^2 \cdot g^{-1}$ and 7.1 $m^2 \cdot g^{-1}$, respectively. It means that the $CaCO_3$ treated porous electrode has less micropores, which contributes much to surface area but little to capacitance, that was proved in other research results[15]. The larger surface area of pores bigger than 2 nm suggests that the P1-PG10 has higher capacitance. The nitrogen adsorption isotherms of PG10 and P1-PG10 electrodes are reflected in Fig. 6E.

The electrochemical performances of the as-prepared porous electrodes were tested. As shown in Fig. 7A, in comparison with the solid PG10 electrode, the P0.5-PG10, P1-PG10 porous electrodes have rectangular and symmetric CV curves, implying their good electrical capacity. Fig. 7B shows the capacitance values of the porous electrode against scan rate. The highest capacitance, 509 $F \cdot g^{-1}$, was obtained using P1-PG10 at scan rate of 0.005 $V \cdot s^{-1}$, which is much higher than that of the solid electrode of PG10 electrode, 359 $F \cdot g^{-1}$, showing clearly that the capacitance depends on the porous ratio. However, when more pores were introduced, the mechanical strength of the porous electrode could be weakened and their electrical conductivity was decreased,

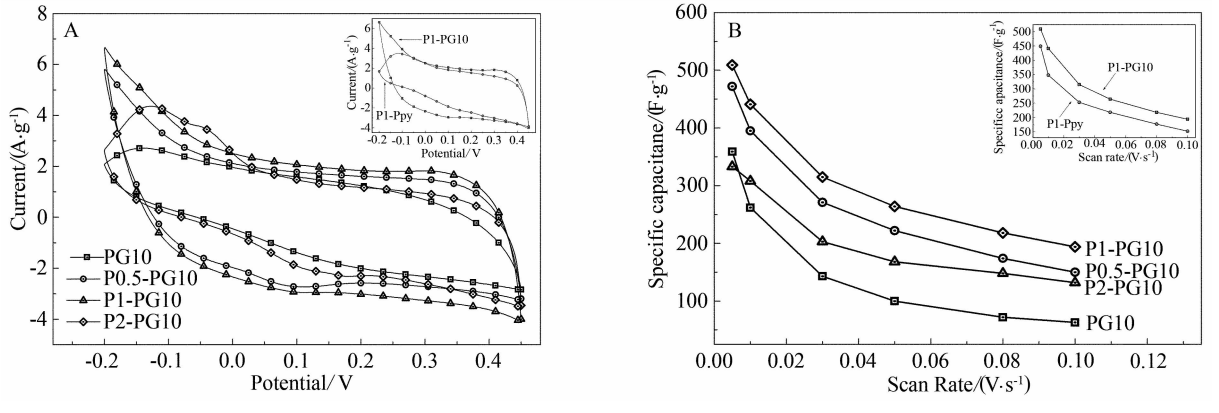

Fig. 7 CV curves of the porous electrodes PG10, P0.5-PG10, P1-PG10, P2-PG10 and P1-Ppy composites obtained at the scan rate of 0.01 $V \cdot s^{-1}$ (A) and the specific capacitances of PG10, P0.5-PG10, P1-PG10, P2-PG10 and P1-Ppy electrodes at various scan rates (B)

thus influenced the final capacitance. For example, the porous electrode P2-PG10 showed only a capacitance of 333 $F \cdot g^{-1}$, which is much lower than P1-PG10. The porous electrode of pure Ppy (P1-Ppy, $CaCO_3$: Ppy = 1∶1), shown in Fig. 7B, was also prepared. The capacitance of the P1-Ppy, 449 $F \cdot g^{-1}$, is higher than that of the solid Ppy electrode, 421 $F \cdot g^{-1}$, but lower than that of the P1-PG10, 509 $F \cdot g^{-1}$. These results showed that the porous Ppy/CRGO electrodes have higher capacitance and, of course, are more suitable for the supercapacitor construction.

The galvanostatic charge-discharge curves of the electrodes with different porosities are shown in Fig. 8A. Comparably, the discharge rate of porous P1-PG10 electrode is much slower than the others, and therefore has the highest capacitance. Fig. 8B shows the specific capacitance of porous electrodes against current density which were calculated using Equation (1). With the increase of current density, the capacitance of all the electrodes decreases. However, the decreasing rates of the electrodes based on the layered Ppy/CRGO composites are much lower than that of the Ppy electrode. These results are in agreement with the CV results.

As illustrated in Fig. 9A and B, the ESR of P1-PG10 electrode is ~1.75 , which is smaller than any other porous PG10 electrodes, revealing that the P1-PG10 electrode assumes better charge and discharge performances. Additionally, the straight part of Nyquist plot at lower frequency region inclines more closely to the imaginary axis (*y*-axis) than the solid PG10, P0.5-PG10, P2-PG10, and P1-Ppy electrodes. The result shows, on the other hand, that the layered motif and high surface area of the porous electrode improves their capacitive behavior. The specific energy and specific power were calculated using galvanostatic charge-discharge data acquired at different current densities (Fig. 8) using Equations (3) and (4), and results are shown in Fig. 9C. The P1-PG10 electrode has the power density of 162.5 $W \cdot kg^{-1}$ and the energy density of 27.8 $Wh \cdot kg^{-1}$ at a current density of 0.25 $A \cdot g^{-1}$, which are higher than those of other electrodes reported in this work. The cycle stability of P1-PG10 electrode at the scan rate of 0.01 $V \cdot s^{-1}$ is shown in Fig. 9D. An increase of capacitance is observed after a decrease in the first 20 cycles, due to the further reduction of the residual oxygen-containing groups in Ppy/CRGO during the electrochemical process, a similar phenomenon was reported by others[6]. After 100 cycles, only 13% of initial capacitance was lost, that shows the P1-PG10 electrode has good cycling stability.

3 Conclusions

We have demonstrated that the Ppy could be grafted on the GO surfaces through *in-situ* polymerization of pyrrole that generates the layered Ppy/CRGO

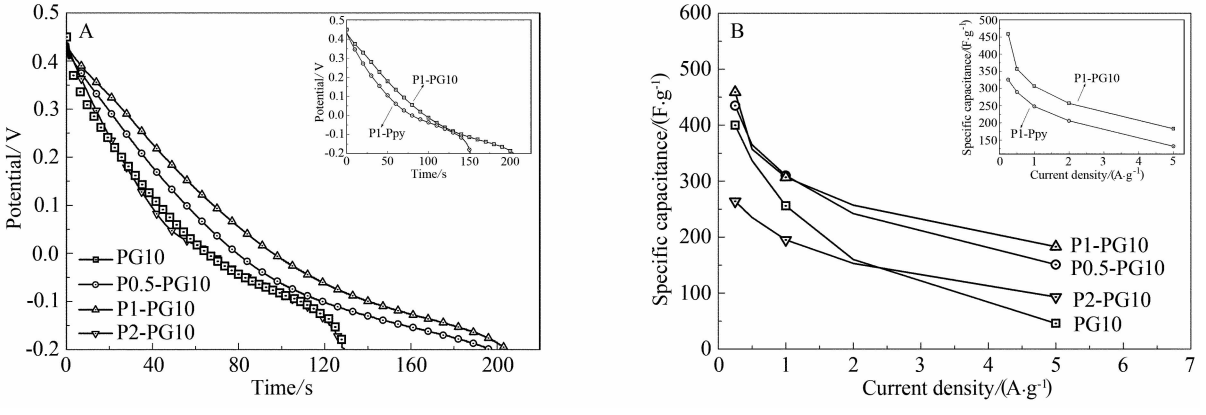

Fig. 8　Galvanostatic charge-discharge curves for PG10, P0.5-PG10, P1-PG10, P2-PG10 and P1-Ppy at current density of 1 $A \cdot g^{-1}$ (A) and the specific capacitances of PG10, P0.5-PG10, P1-PG10, P2-PG10 and P1-Ppy electrodes at various current densities (B)

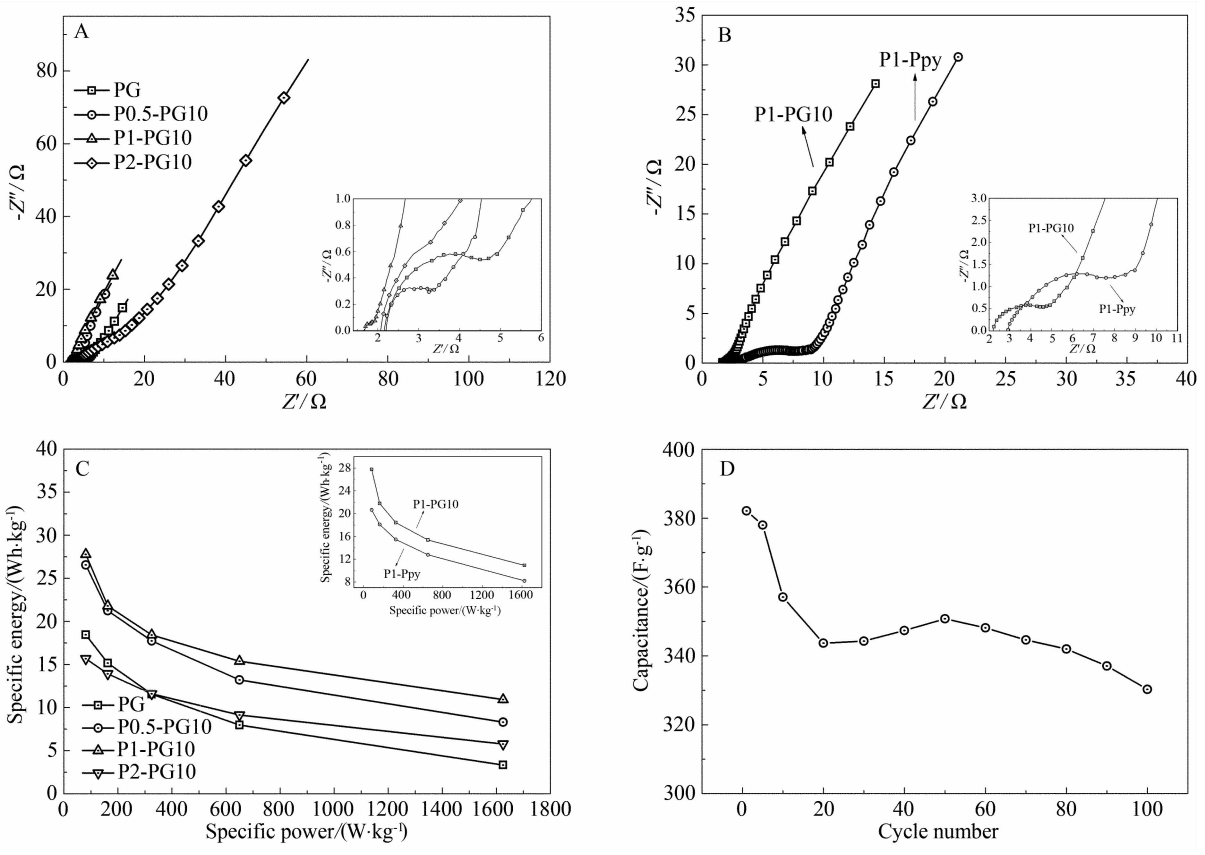

Fig. 9 Nyquist plots of solid PG10, P0.5-PG10, P1-PG10, P2-PG10 (A), Nyquist plots of P1-PG10 and P1-Ppy electrodes (B), ragon plots of solid PG10, P0.5-PG10, P1-PG10, P2-PG10 and P1-Ppy electrodes (C) and cycling stability of P1-PG10 electrode from the 1st to the 100th cycle at the scan rate of $0.01 V \cdot s^{-1}$ (D)

composites. The as-prepared layered composites show better electrical conductivity, thermal stability and electrochemical properties than those of the individual Ppy and GO. Both solid and porous electrodes were fabricated using the layered Ppy/CRGO composites and their electrochemical performances have been studied systematically. It has been illustrated that by controlling the composition (the mass ratio of Ppy to CRGO) and introducing the proper pores within the electrodes, the electrical capacitance of Ppy/CRGO electrode was enhanced dramatically. Given the simple preparation procedures and pronounced electrochemical performances, the porous Ppy/CRGO electrodes may find application in supercapacitors or other electrical devices.

References:

[1] Jeong Y U, Manthiram A. Nanocrystalline manganese oxides for electrochemical capacitors with neutral electrolytes[J]. Journal of the Electrochemical Society, 2002, 149(11): A1419-A1422.

[2] Devine-Wright P. Beyond NIMBYism: Towards an integrated framework for understanding public perceptions of wind energy[J]. Wind Energy, 2005, 8(2): 125-139.

[3] Manwell J F, McGowan J G, Rogers A L. Wind energy explained: Theory, design and application[M]. Amherst: John Wiley and Sons, 2002: 11-22.

[4] Kim J Y, Lee K, Coates N E, et al. Efficient tandem polymer solar cells fabricated by all-solution processing[J]. Science, 2007, 317(5835): 222-225.

[5] O'regan B, Grätzel M. A low-cost, high-efficiency solar cell based on dye-sensitized colloidal TiO_2 films[J]. Nature, 1991, 353(6346): 737-740.

[6] Zhang D, Zhang X, Chen Y, et al. Enhanced capacitance and rate capability of graphene/polypyrrole composite as electrode material for supercapacitors[J]. Journal of Power Sources, 2011, 196(14): 5990-5996.

[7] Conway B E. Electrochemical supercapacitors: Scientific fundamentals and technological applications[M]. New York: Springer, 1999: 444-445.

[8] Fuertes, A B, Lota G, Centeno T A, et al. Templated mesoporous carbons for supercapacitor application [J]. Electrochimica Acta, 2005, 50(14): 2799-2805.

[9] Conway B E. Transition from "supercapacitor" to "battery" behavior in electrochemical energy storage [J]. Journal of the Electrochemical Society, 1991, 138(6): 1539-1540.

[10] Stoller M D, Park S, Zhu Y, et al. Graphene-based ultracapacitors[J]. Nano Letters, 2008, 8(10): 3498-3502.

[11] Lota G, Lota K, Frackowiak E. Nanotubes based composites rich in nitrogen for supercapacitor application [J]. Electrochemistry Communications, 2007, 9(7): 1828-1832.

[12] Subramanian V, Zhu H, Vajtai R, et al. Hydrothermal synthesis and pseudocapacitance properties of MnO_2 nanostructures[J]. The Journal of Physical Chemistry B, 2005, 109(43): 20207-20214.

[13] Bose S, Kim N H, Kuila T, et al. Electrochemical performance of a graphene-polypyrrole nanocomposite as a supercapacitor electrode[J]. Nanotechnology, 2011, 22(29): 295202-295210.

[14] Gamby J, Taberna P L, Simon P, et al. Studies and characterisations of various activated carbons used for carbon/carbon supercapacitors [J]. Journal of Power Sources, 2001, 101(1): 109-116.

[15] Lozano-Castelló D, Cazorla-Amorós D, Linares-Solano A, et al. Influence of pore structure and surface chemistry on electric double layer capacitance in non-aqueous electrolyte[J]. Carbon, 2003, 41(9): 1765-1775.

[16] Frackowiak E. Carbon materials for supercapacitor application[J]. Physical Chemistry Chemical Physics, 2007, 9(15): 1774-1785.

[17] Prabaharan S R S, Vimala R, Zainal Z. Nanostructured mesoporous carbon as electrodes for supercapacitors [J]. Journal of Power Sources, 2006, 161(1): 730-736.

[18] Li W, Chen D, Li Z, et al. Nitrogen enriched mesoporous carbon spheres obtained by a facile method and its application for electrochemical capacitor[J]. Electrochemistry Communications, 2007, 9(4): 569-573.

[19] An K H, Kim W S, Park Y S, et al. Electrochemical properties of high-power supercapacitors using single-walled carbon nanotube electrodes [J]. Advanced Functional Materials, 2001, 11(5): 387-392.

[20] Niu C, Sichel K E, Hoch R, et al. High power electrochemical capacitors based on carbon nanotube electrodes[J]. Applied Physics Letters, 1997, 70(11): 1480-1482.

[21] Wang Y, Shi Z, Huang Y, et al. Supercapacitor devices based on graphene materials[J]. The Journal of Physical Chemistry C, 2009, 113(30): 13103-13107.

[22] Kötz R, Carlen M. Principles and applications of electrochemical capacitors[J]. Electrochimica acta, 2000, 45(15/16): 2483-2498.

[23] Zhou H, Chen H, Luo S, et al. The effect of the polyaniline morphology on the performance of polyaniline supercapacitors[J]. Journal of Solid State Electrochemistry, 2005, 9(8): 574-580.

[24] Gupta V, Miura N. High performance electrochemical supercapacitor from electrochemically synthesized nanostructured polyaniline [J]. Materials Letters, 2006, 60(12): 1466-1469.

[25] Ingram M D, Staesche H, Ryder K S. 'Activated' polypyrrole electrodes for high-power supercapacitor applications[J]. Solid State Ionics, 2004, 169(1/4): 51-57.

[26] Sharma R K, Rastogi A C, Desu S B. Pulse polymerized polypyrrole electrodes for high energy density electrochemical supercapacitor [J]. Electrochemistry Communications, 2008, 10(2): 268-272.

[27] Laforgue A, Simon P, Sarrazin C, et al. Polythiophene-based supercapacitors [J]. Journal of Power Sources, 1999, 80(1/2): 142-148.

[28] Xu, J, Wang K, Zu S, et al. Hierarchical nanocomposites of polyaniline nanowire arrays on graphene oxide sheets with synergistic effect for energy storage[J]. ACS Nano, 2010, 4(9): 5019-5026.

[29] Zhang K, Zhang L, Zhao X S, et al. Graphene/polyaniline nanofiber composites as supercapacitor electrodes [J]. Chemistry of Materials, 2010, 22(4): 1392-1401.

[30] Zhang J, Yang H, Shen G, et al. Reduction of graphene oxide vial-ascorbic acid[J]. Chemical Communications, 2009, 46(7): 1112-1114.

[31] Zhou X, Zhang J, Wu H, et al. Reducing graphene oxide via hydroxylamine: A simple and efficient route to graphene[J]. The Journal of Physical Chemistry C, 2011, 115(24): 11957-11961.

[32] He C, Yang C, Li Y. Chemical synthesis of coral-like nanowires and nanowire networks of conducting polypyrrole[J]. Synthetic Metals, 2003, 139(2): 539-

545.

[33] Amarnath C A, Hong C E, Kim N H, et al. Efficient synthesis of graphene sheets using pyrrole as a reducing agent[J]. Carbon, 2011, 49(11): 3497-3502.

[34] Stankovich S, Dikin D A, Dommett G H B, et al. Graphene-based composite materials[J]. Nature, 2006, 442(7100): 282-286.

[35] Li D, Muller M B, Gilje S, et al. Processable aqueous dispersions of graphene nanosheets[J]. Nature Nanotechnology, 2008, 3(2): 101-105.

[36] Liu C, Yu Z, Neff D, et al. Graphene-based supercapacitor with an ultrahigh energy density[J]. Nano Letters, 2010, 10(12): 4863-4868.

聚吡咯/氧化石墨烯层状复合材料的制备及其在超级电容器中的应用

许思哲, 周雪皎, 吴 坤, 杨永强, 吴海霞*

(上海交通大学微纳米科学与技术研究院, 上海 200240)

摘要: 通过将吡咯单体在低温下与氧化石墨烯进行原位聚合,获得聚吡咯/石墨烯(Ppy/CRGO)复合材料. 采用场发射电子显微镜(FESEM)、红外 (FT-IR)和热重分析(TGA)对复合物的表面形貌、结构进行表征. FESEM 结果表明,通过控制氧化石墨烯(GO)和吡咯单体的质量比例,可以对复合物的层状和厚度进行调控. FT-IR 和 TGA 结果表明,聚吡咯(Ppy)是通过化学键合的方式与氧化石墨烯复合在一起. 通过机械冷压法将粉末状 Ppy/CRGO 复合物压成圆片电极,并探讨了石墨烯和聚吡咯复合比例、反应时间、烘干温度和孔隙率等因素对 Ppy/CRGO 复合物电极的电学和电化学性能的影响. 结果表明,Ppy 与 CRGO 质量比为 10∶1 所制得的 Ppy/CRGO 复合物的电容量为 421 $F \cdot g^{-1}$,通过在电极中引入孔隙,电容量能进一步提升为 509 $F \cdot g^{-1}$.

关键词: 氧化石墨烯; 化学还原石墨烯; 聚吡咯; 复合物; 超级电容器